

Influence of Oxygen on the Kinetics of Omega and Alpha Phase Formation in Beta Ti–V



ROBERT JOSEF ENZINGER, MARTIN LUCKABAUER, NORIHIKO L. OKAMOTO, TETSU ICHITSUBO, WOLFGANG SPRENGEL, and ROLAND WÜRSCHUM

A detailed understanding of the kinetics of phase formation in β -stabilised titanium is of decisive importance for the applicability of these materials. However, the complex nature and long timescales of the various transformations, calls for specialized measurement techniques. In this work high-stability isothermal laser dilatometry is used to study the temporal volume changes associated with the various phase formation processes. Distinctly different behaviours between samples of Ti–21 at. pct V with different solute oxygen content could be detected and quantified. Temperature regimes for both diffusionless and diffusion-assisted isothermal ω -formation as well as for ω -to- α -transformation were determined. Low oxygen contents promote the diffusionless ω -formation mechanism, but retard the diffusion-assisted one as well as the ω -to- α -transformation process. The results confirm recent findings of a clear distinction between the diffusionless and diffusion-assisted isothermal ω formation modes. Modelling of the ω -phase formation applying Austin–Rickett kinetics revealed the temperature-dependent formation rates, on the basis of which the isothermal TTT-diagrams were developed which reflect the strong influence of the oxygen content.

<https://doi.org/10.1007/s11661-022-06881-1>
© The Author(s) 2022

I. INTRODUCTION

DURING the last decades, β -Ti-alloys have attracted growing attention in various branches of industry, since they provide a unique combination of material properties. Besides a low mass density at simultaneously high strength, this includes an excellent corrosion resistance as well as a good cold processability.^[1–3] These properties mainly arise from microstructures containing proportions of the more loosely packed high-temperature β -Ti-phase (bcc) which is stabilised at ambient temperature by the addition of alloying elements like Ta, Mo, Nb, and V, called β -stabilisers.^[4]

However, the formation of the metastable nanoscale ω -phase in this alloy class has been a long-standing problem due to its deteriorating influence on mechanical

properties.^[5,6] This phase mainly appears upon heat-treating alloys with a low β -stabiliser content. These kind of alloys are favourable for reasons of lower costs and mass density. In order to exploit their full potential, strategies are therefore required to controllably transform the ω -phase into other phases or to even suppress its formation completely.^[7–9] For this reason, there is a great need for investigation methods yielding novel insight into phase transformation in these alloys.

Recent advances make dilatometry a powerful tool for exactly this purpose.^[10,11] Based on our previous studies of dilute Al alloys,^[12,13] high-precision isothermal dilatometry is applied in the present work on Ti–V-alloys.

Figure 1 shows the phase diagram for the Ti–V-alloy system both without oxygen and with a finite amount of oxygen which is an inevitable constituent in Ti-alloys used in practice.^[14,15] The oxygen-containing alloy (red dashed lines) is characterised by a monotectic reaction, where the β -phase decomposes into V-lean and V-rich regions, denoted as β_1 and β_r .

The above-mentioned formation of the metastable ω -phases for low β -stabiliser contents occurs around the so-called athermal transformation line T_{ath} (see Figure 1, red dash-dotted curve), which represents a limiting curve for the stability of the β -phase.^[18] The ideal ω -phase can be considered as a complete collapse of neighbouring $[111]_{\beta}$ -lattice plane pairs yielding a hexagonal crystal structure with the lattice constants

ROBERT JOSEF ENZINGER, WOLFGANG SPRENGEL, and ROLAND WÜRSCHUM are with the Institute of Materials Physics, Graz University of Technology, Petersgasse 16, Graz, 8010, Austria. MARTIN LUCKABAUER is with the Faculty of Engineering Technology, University of Twente, Enschede, 7522LW, The Netherlands. NORIHIKO L. OKAMOTO and TETSU ICHITSUBO are with the Institute for Materials Research, Tohoku University, Sendai, Miyagi 980-8577, Japan. Contact e-mail: wuerschum@tugraz.at

Manuscript submitted May 2, 2022; accepted October 23, 2022.

Article published online November 30, 2022

being related to that of β -phase lattice constants ($a_\omega = \sqrt{2}a_\beta$, $c_\omega = \frac{\sqrt{3}}{2}a_\beta$, see Figure 2).^[17,19] In most cases, however, not the immediate formation of the ideal ω -phase occurs, but rather intermediate versions with respect to the degree of lattice plane collapse.

Concomitantly, the ω -phase has no fixed composition but is known to eject β -stabiliser into its surroundings exchanging it by Ti.^[20]

Regarding the ω -formation process, a (*diffusion-assisted*) isothermal and an *athermal* mode are traditionally distinguished,^[5] which have just recently been supplemented by a *diffusionless-isothermal* mode^[17,18]:

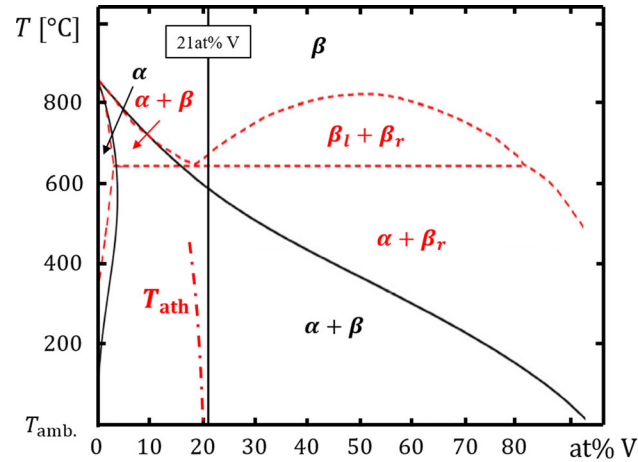


Fig. 1—Phase diagram of Ti–V-alloy system for zero oxygen content (black solid lines) and for finite oxygen content (red dashed lines) redrawn from Ref.[16]. Phases α , β , β_l , β_r , where the latter denote V-lean and V-rich, respectively. The dash-dotted red curve marks the athermal transformation curve T_{ath} (adopted from Ref.[17]), the vertical black line the composition of the present studies (Color figure online).

i. Diffusion-assisted formation of the ω -phase under isothermal conditions, denoted henceforth ω_{iso} , occurs during isothermal ageing in the phase region notably above T_{ath} and at sufficiently high temperatures for diffusion to occur. Here, the decomposition process of the β -phase is found to play a crucial role, since it steadily produces new β -stabiliser lean regions which are able to transform to the ω -phase.

ii. Athermal ω -phase formation (ω_{ath}) occurs upon undershooting T_{ath} during quenching. Here, nanoscale regions with the same composition as the parent bcc phase transform to the ω -phase. This transformation mode is usually found to be completely reversible.^[19]

iii. The diffusionless-isothermal formation of ω , which will be denoted $\omega_{dl,iso}$ in the following, prevails during isothermal ageing at low temperatures, insufficient for diffusion to occur, and when the alloy is located in the phase region slightly above the T_{ath} -curve after

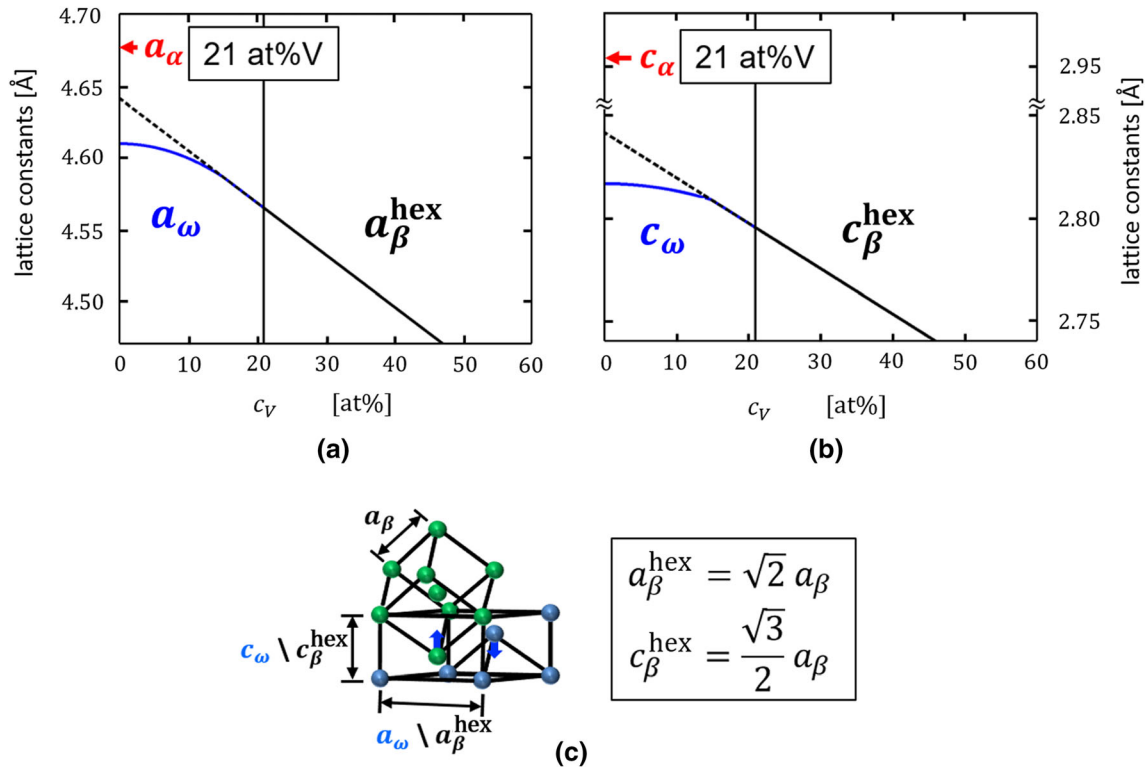


Fig. 2—(a, b) Lattice constants of bcc β -phase (Eq. [A4]) in hexagonal representation (black) and of the hexagonal ω -phase (blue) (Eqs. [A8a] and [A8b]) in dependence of V-concentration c_V as well as lattice constants of c_V -independent hcp α -phase (red arrows) (Eqs. A12a and A12b). (c) bcc and hexagonal unit cell of the β -phase along with the relations for the lattice constant a_β of cubic β in hexagonal representation (a_β^{hex} , c_β^{hex}) (Color figure online).

quenching. The ω -phase formation is known to start at the regions slightly more depleted in β -stabiliser than their surroundings, thus in regions which are already below their local temperature threshold for athermal ω -phase formation. The inhomogeneous nano-scale β -stabiliser distribution is a consequence of quenched in equilibrium concentration fluctuations that are inevitably present in the alloy after quenching from the solution annealing temperature.^[17,18]

After the description of the experimental procedure (Section II) and the presentation of the experimental results (Section III-A), a model will be developed that allows to relate the various transformation processes with specific length change (Section III-B) and in this way to derive information about microscopic changes based on the dilatometry measurements (Section III-C). Finally, in Section IV, kinetic modeling is applied to deduce temperature-dependent formation rates for the ω -formation process, which will allow to construct the isothermal time-temperature-transformation (TTT)-diagram. In the wake of the comprehensive studies, presented here, preliminary parts of the ω_{iso} -formation were communicated at a conference.^[21]

II. EXPERIMENTAL

Two Ti-V-samples with a nominal composition of 21 at. pct V (see Figure 1, vertical black line) and different oxygen contents were investigated following the procedure described elsewhere.^[22] For this purpose, two sets of starting materials were prepared by arc-melting and tilt-casting, *i.e.*, a less pure set (Ti: 99.9 wt pct, V: 99.7 wt pct) and a high-purity set (Ti: 99.999 wt pct, V: 99.7 wt pct) with an oxygen content lower than 0.1 at. pct. The Ti- and V-contents of the alloy samples were determined by inductively coupled plasma-optical emission spectrometry (ICP-OES, IRIS Advantage DUO, Thermo Fisher Scientific Inc., USA), the oxygen by an oxygen/nitrogen elemental analyser (TC-436, LECO Corp., USA). The less pure sample exhibits a V-content of 20.9 at. pct and an O-content of about 1 at. pct, the latter of which is common for titanium alloys and which therefore will be denoted the “sample with a regular oxygen content”. The high-purity sample with a V-content of 21.3 at. pct V contains only about one tenth of the oxygen content (*ca.* 0.1 at. pct O) compared to the first one, and correspondingly will be referred to as the “sample with strongly reduced oxygen content” or with the extension HP for high-purity (Ti21.3V(HP)). Right after their production, the samples were subjected to a solution treatment at 800 °C for 2 hours at a pressure of 1.0×10^{-5} mbar, followed by quenching in ice water. This was done in order to avoid any irreversible processes disturbing the investigations of phase formation processes taking place at ageing temperatures substantially lower than 800 °C.

For the dilatometric measurements cylindrical-shaped samples with a diameter of 5.6 mm and a length of 20.0 mm were used. Dilatometric measurements were performed for various ageing temperatures in the range of 41 °C to 450 °C for Ti20.9V, respectively 100 °C to 450 °C for Ti21.3V(HP), under high vacuum conditions (1.0×10^{-5} mbar) using the laser dilatometer described in detail elsewhere.^[10] Prior to each measurement, the samples were solution annealed in situ at 880 °C until length did not change anymore, which took at least 45 min and which was considered as evidence to have attained a state with β -phase, exclusively. Direct quenching to the respective ageing temperatures was performed in a He-gas stream yielding a quenching rate of approximately 35 K s^{-1} . After every second measurement, an ageing measurement at 300 °C was conducted. By checking its congruency with the preceding ageing measurements recorded at this temperature, any device-related errors, long-term effects or irreversible changes of the sample could be excluded.

III. EXPERIMENTAL RESULTS, LENGTH CHANGE MODELING, AND ANALYSIS

A. Experimental Results

The relative length changes $\Delta L/L_0$ measured upon isothermal annealing of the Ti-V-samples with different oxygen content are summarised in Figure 3. In the temperature range below 400 °C, contraction, *i.e.*, a negative relative length change, occurs, which increases in absolute value with increasing temperature up to $T = 300$ °C (see Figures 3(a) and (b)) and decreases above (Figures 3(c) and (d)). For $T = 400$ °C and 450 °C, an expansion is superimposed, which is by far more pronounced in case of the sample with a regular oxygen content (see 400 °C in Figure 3(c)).

The different behaviour of the two samples are exemplary compared in Figure 3(e) for different temperatures. For $T < 250$ °C, the contraction for the Ti20.9V-sample is smaller than that of the Ti21.3V(HP)-sample, in the range of 250 °C to 300 °C more or less the same, and for $T > 300$ °C larger.

B. Length Change Modeling of Underlying Microstructural Processes

In order to associate the pronounced dilatometric length changes upon annealing (Figure 3) with the underlying microstructural changes, the three elementary processes, *i.e.*, mere *decomposition*, *ω -phase formation*, and *ω -to- α -transformation* are considered in the following. It turns out that each process is characterised by a specific length change behaviour, making dilatometry measurements a unique tool for an in-depth analysis of these processes. The results for these processes are presented in this subsection, the derivation of the models is given in the Appendix A.

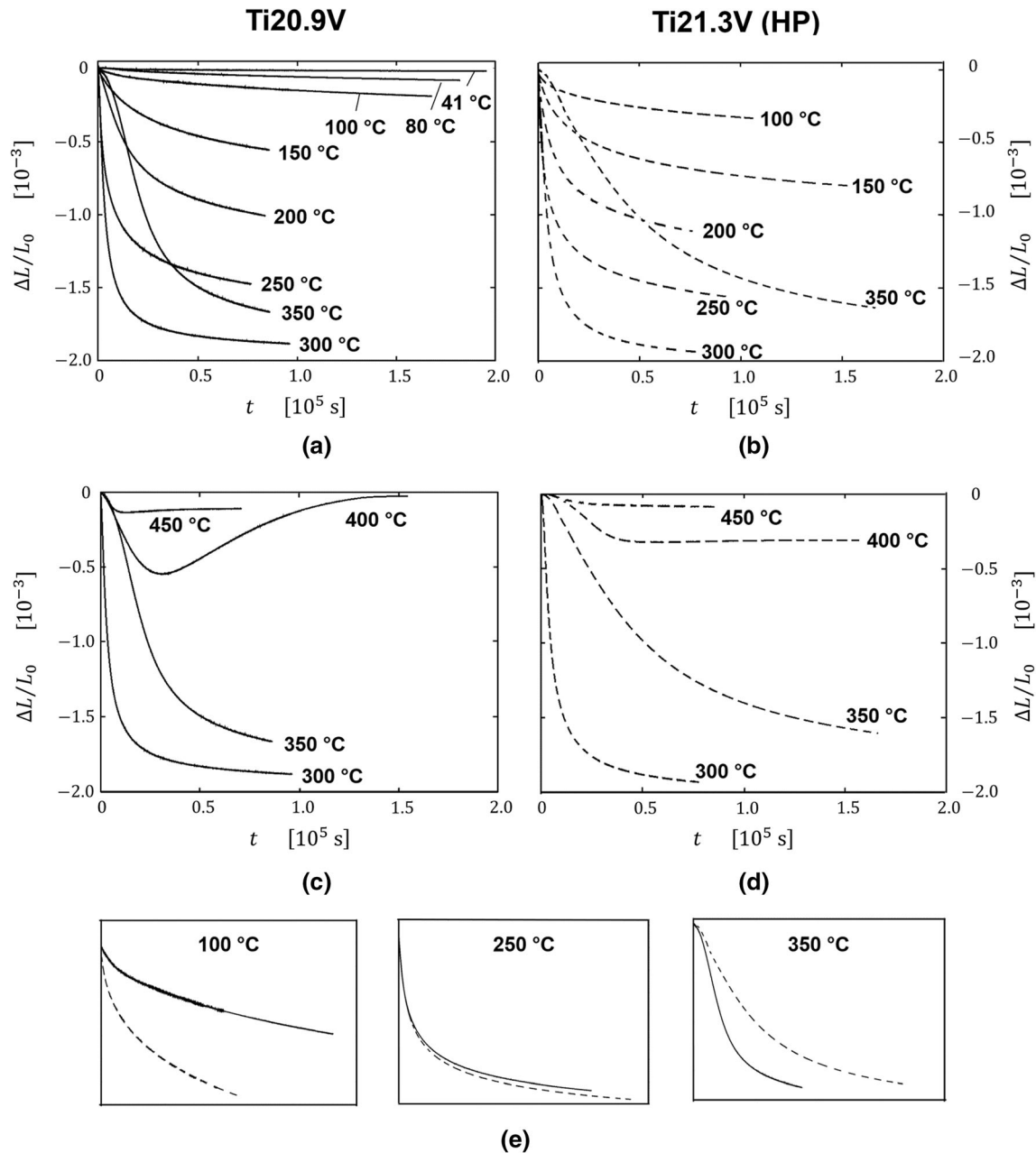


Fig. 3—Relative length change $\Delta L/L_0$ measured over time t upon isothermal ageing at various temperatures for the sample with a regular oxygen content (*a*, *c*; full lines, Ti20.9V) and for the sample with a strongly reduced oxygen content (*b*, *d*; dashed lines, Ti21.3V(HP)). *e* Comparison of the two samples for selected temperatures. L_0 : total sample length at T_{amb} .

1. Decomposition

Decomposition means that V-lean (β_l) and V-rich regions (β_r) are generated by respective diffusional fluxes of V- and Ti-atoms, starting from a compositional profile with a mean V-concentration of $c_{V,0}$. The regions enriching in vanadium are denoted in the following also as *matrix*. During the decomposition process, the sample is assumed to remain entirely in β -phase. The V-lean part (β_l) and the V-enriched matrix (β_r) are characterized by their respective V-concentration (c_{V,β_l} , c_{V,β_r}) and mole fraction (x_{β_l} , x_{β_r}), for which the relations (Eqs. [A7a] and [A7b]) hold. For the relative length

change arising from this decomposition process, one obtains (see Appendix A):

$$\begin{aligned} \left(\frac{\Delta L}{L_0}\right)_{\text{decomp.}} &= \frac{1}{3}x_{\beta_l} \left(\frac{a_{\beta}^3(c_{V,\beta_l}, T)}{a_{\beta}^3(c_{V,0}, T)} - 1 \right) \\ &\quad + \frac{1}{3}x_{\beta_r} \left(\frac{a_{\beta}^3(c_{V,\beta_r}, T)}{a_{\beta}^3(c_{V,0}, T)} - 1 \right) \quad [1] \\ &= \left(\frac{\Delta L}{L_0}\right)_{\beta_l} + \left(\frac{\Delta L}{L_0}\right)_{\beta_r}, \end{aligned}$$

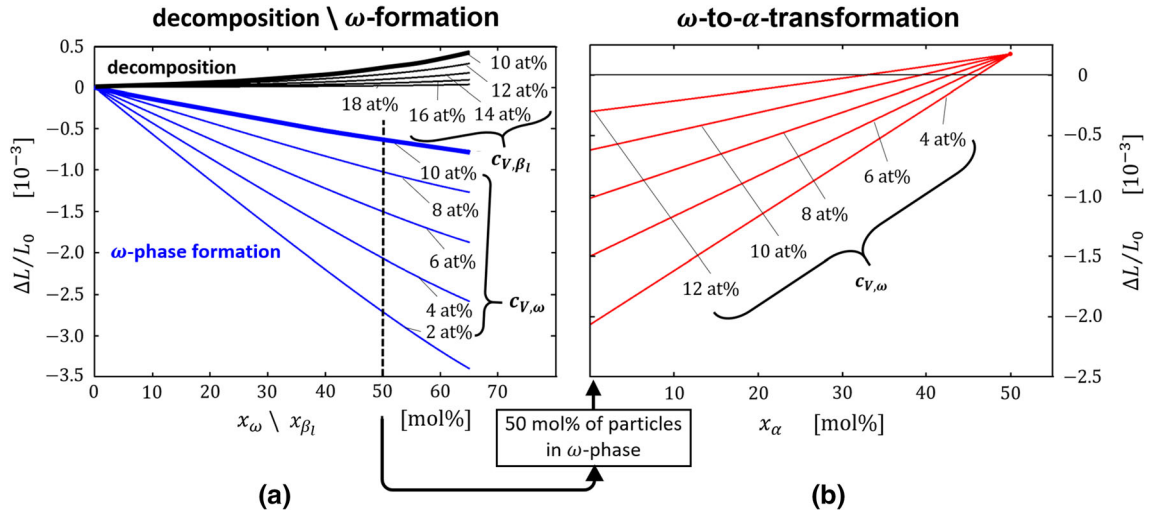


Fig. 4—Length changes calculated for (a) decomposition (black curves) according to Eq. [1], (a) ω -phase formation (blue curves) according to Eq. [2] and for (b) ω -to- α -transformation (red curves) according to Eq. [3]. The calculations have each been performed in dependence of the mole fraction of the V-lean part and for different V-contents in this part (Color figure online).

where a_β denotes the lattice constant of the bcc β -phase. The lattice constant a_β is a function of the temperature T and decreases linearly with increasing V-content (see Eq. [A4]) as shown in Figure 2(a) (black line).

The relative length change with progressive decomposition, *i.e.*, with increasing phase fraction x_{β_l} , according to Eq. [1] is shown in Figure 4(a) (black lines) for different V-contents c_{V,β_l} . As can be seen, the length changes calculated are slightly positive in each case, meaning, the swelling of the V-depleting regions slightly surpasses the contraction of the V-enriching regions. The overall length change associated with decomposition is small due to the linear variation of a_β with c_V .

2. Isothermal omega-phase formation

Starting from the β -phase, V-lean ω -phase particles of hexagonal lattice structure are formed embedded in a V-enriched β -phase matrix, those particles may nucleate in regions depleted in vanadium in the initial phase of the decomposition process. In analogy to the preceding case, the ω -phase and the V-enriched matrix (β_r) are characterized by their respective V-concentration ($c_{V,\omega}$, c_{V,β_r}) and mole fraction (x_ω , x_{β_r}), for which the relations Eqs. [A11a] and [A11b] hold. The relative length change in the case of ω -phase formation reads (see Appendix A):

$$\begin{aligned} \left(\frac{\Delta L}{L_0}\right)_{\omega\text{-form.}} &= \frac{1}{3}x_\omega \left(\frac{\frac{1}{3}\frac{\sqrt{3}}{2}a_\omega^2(c_{V,\omega}, T)c_\omega(c_{V,\omega}, T)}{\frac{1}{2}a_\beta(c_{V,0}, T)} - 1 \right) \\ &\quad + \frac{1}{3}x_{\beta_r} \left(\frac{a_\beta^3(c_{V,\beta_r}, T)}{a_\beta^3(c_{V,0}, T)} - 1 \right) \\ &= \left(\frac{\Delta L}{L_0}\right)_\omega + \left(\frac{\Delta L}{L_0}\right)_{\beta_r}, \end{aligned} \quad [2]$$

where a_ω , c_ω denote the lattice constants of the hexagonal ω -phase, and a_β that of the β -matrix. As shown in Figures 2(a) and (b) (blue lines), the lattice constants a_ω (Eq. [A8a]) and c_ω (Eq. [A8b]) increase with decreasing V-concentration, but bend when approaching low V-contents. This means that below a certain concentration threshold ω -phase particles will have a smaller volume than the vanadium enriched β -matrix they substitute.

The resulting relative length change with increasing ω -phase formation according to Eq. [2] is shown in Figure 4(a) for different V-contents $c_{V,\omega}$ of the ω -phase particles (blue lines). In contrast to the decomposition process, the length decreases upon ω -phase formation, since in this case, due to the aforementioned bending of $a_\beta(c_V)$ and $c_\beta(c_V)$, the expansion associated with V-lean part, *i.e.*, the ω -phase particles, is smaller than the contraction of the V-enriched β -matrix.

3. Diffusionless-isothermal omega-phase formation

At temperatures below a certain threshold value the ω -phase particles will form through the diffusionless-isothermal mechanism. In this regime the formation of ω particles in depleted regions is the only process to consider. As can be seen in Figure 2 the lattice constants of the ω phase are smaller than those of the β phase below about 15 at. pct vanadium. The relative length change given above (Eq. [2]) holds for this case as well. In Figure 4 the expected length changes for different mole fractions of ω phase with different compositions is shown. As will be analyzed in Section III-C, the isothermal (ω_{iso}) and diffusion-less isothermal ω -phase formation ($\omega_{dl,iso}$) can be distinguished by means of the decomposition preceding the ω_{iso} -formation, but not the $\omega_{dl,iso}$ -formation.

4. Omega-to-alpha-transformation

In contrast to the mesoscopically homogeneous β -phase as starting condition for the two above-mentioned processes, the ω -to- α -transformation starts from a state where V-lean ω -phase particles, with initial fraction x_ω^0 and V-content $c_{V,\omega}^0$, are embedded in a V-enriched β matrix. Upon ω -to- α -transformation, the β -matrix fraction x_β^0 is considered to be constant, however, an ejection of V-atoms from the transforming particles into the β -matrix occurs since the solubility for vanadium in the α -phase is negligibly small compared to that in the ω -phase ($c_{V,\omega}^0$). Again, there are relations between the mole fractions and concentrations of the different regions included in the transformation process, Eqs. [A14a], [A14b], and [A14c]. For the relative length changes associated with the ω -to- α -transformation, one obtains (see Appendix A):

$$\begin{aligned} \left(\frac{\Delta L}{L_0}\right)_{\omega\text{-to-}\alpha\text{-transform.}} &= \frac{1}{3}x_\alpha \left(\frac{\frac{1}{2}\sqrt{3}a_\alpha^2(T)c_\alpha}{\frac{1}{2}a_\beta^3(c_{V,0}, T)} - 1 \right) \\ &+ \frac{1}{3}(x_\omega^0 - x_\alpha) \left(\frac{\frac{1}{2}\sqrt{3}a_\omega^2(c_{V,\omega}^0, T)c_\omega(c_{V,\omega}^0, T)}{\frac{1}{2}a_\beta^3(c_{V,0}, T)} - 1 \right) \\ &+ \frac{1}{3}x_\beta^0 \left(\frac{a_\beta^3(c_{V,\beta}, T)}{a_\beta^3(c_{V,0}, T)} - 1 \right) \quad [3] \\ &= \left(\frac{\Delta L}{L_0}\right)_\alpha + \left(\frac{\Delta L}{L_0}\right)_\omega + \left(\frac{\Delta L}{L_0}\right)_\beta. \end{aligned}$$

In Eq. [3], a_α (Eq. [A12a]) and c_α (Eq. [A12b]) denote the lattice constants of the emerging hcp- α -phase, for which only the temperature dependence is considered but not any variation with V-content due to the minor V-solubility. The lattice constants of the α -phase exceed by far those of the ω -phase, it substitutes (see red arrows in Figures 2(a) and (b)).

Figure 4(b) shows the variation of the relative length change for a growing α -phase fraction according to Eq. [3] assuming an initial fraction $x_\omega^0 = 50$ pct of the ω -phase at various V-concentrations $c_{V,\omega}^0$. Note that the initial $\Delta L/L_0$ -values are negative since all length changes are referred to the homogenous initial β -phase. As can be clearly seen, the ω -to- α -transformation leads to a strong positive length change which arises from the aforementioned larger lattice constants of the almost vanadium free α - compared to the vanadium containing ω -phase. For high α -phase fractions, the expansion associated with the α -phase formation even exceeds the contraction of the β -matrix due to V-enrichment resulting in a net increase ($\Delta L/L_0 > 0$) in comparison to the initial β -phase.

To sum up the three processes, ω -formation leads to strongly negative length changes and ω -to- α -transformation to strongly positive length changes, whereas the length change associated with decomposition is comparatively small.

C. Analysis of Measurements

In this subsection, the measured dilatometric length changes (Figure 3) are associated with the length changes calculated for the three processes expected to occur (Figure 4).

1. Identification of phase regions

As stated in the introduction, two different modes of ω -formation are commonly found to occur at low and intermediate ageing temperatures, the diffusionless and the diffusion-assisted isothermal mechanism, $\omega_{dl,iso}$ and ω_{iso} . Since the diffusion-assisted version requires preceding decomposition, in contrast to $\omega_{dl,iso}$ -formation, the distinctly different length change behaviour of decomposition and ω -formation (Figure 4(a)) may allow to distinguish between the $\omega_{dl,iso}$ - and ω_{iso} -processes. For the ω_{iso} -formation, the slight positive length changes associated with decomposition should result in an initial plateau region before the strong negative length change due to ω -phase formation starts to dominate. This initial behaviour can at best be assessed by considering the time derivative of the length change curves as shown in Figure 5(e). The tiny positive length changes caused by initial decomposition reduce the strong negative length changes caused by ω -phase formation and manifest themselves in an intensified bending of the time derivative the y -axis. In Figure 5(e), such bending is observed in case of ageing at 200 °C and 250 °C when being compared to ageing at 150 °C (blue rectangle). For ageing at 300 °C and 350 °C, even a minimum can be seen, which is caused by the same mechanism (blue ellipse in Figure 5(e)). The lack of such a minimum or bending for ageing at 150 °C clearly shows that decomposition is *not* involved at all at this temperature. Therefore, the boundary is set to lay around 200 °C, *i.e.*, below this temperature $\omega_{dl,iso}$ -formation gets predominant and above ω_{iso} -formation, with increasing intensity towards lower and higher temperatures, respectively. For the sample with reduced oxygen content, a similar analysis by means of the time derivative (not shown) yields the same result concerning the transition from $\omega_{dl,iso}$ - to ω_{iso} -formation. The regions, where $\omega_{dl,iso}$ - and ω_{iso} -formation take place are marked in Figure 5 in green and light blue, respectively. A region of mere decomposition can hardly be discerned in the length change measurements.

Concerning the ω -to- α -transformation, this process has been shown to be connected with strong length increase (Figure 4b) (partially) reverting the length decreases due to ω -formation. Such behaviour becomes clearly visible for both samples upon ageing at 400 °C and higher temperatures. The respective regions have been marked in Figure 5 in red.

2. Influence of oxygen

In the temperature range, where $\omega_{dl,iso}$ -formation is observed, the variations in length per unit time are in any case larger for the sample with reduced oxygen content (Figure 3(e)). That means, this mode of ω -formation proceeds faster, *i.e.*, according to Eq. [2], a larger fraction of ω -phase is formed per unit time and/or the V-content of the ω -phase particles present is dropping faster. Similar observations have been reported by Okamoto *et al.*,^[22] who investigated the influence of the oxygen content on the $\omega_{dl,iso}$ -formation mode by a couple of other techniques.

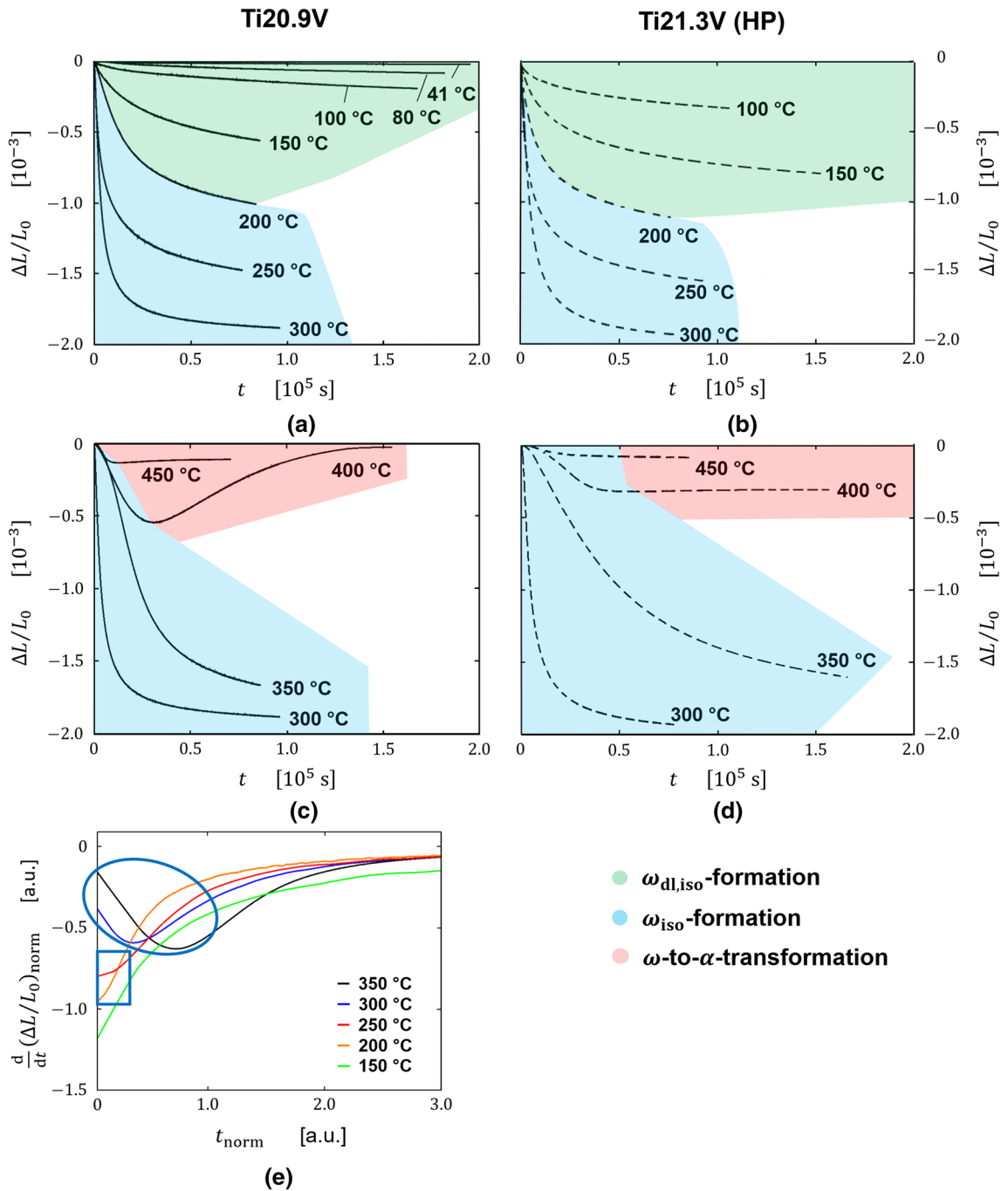


Fig. 5—Correlation between the measured length changes (Fig. 3) and the underlying transformation processes for the sample with regular oxygen content (a, c) and the sample with strongly reduced oxygen content (b, d). The phase regions (time, temperature), where $\omega_{dl,iso}$ -, ω_{iso} -, and α -phase formation take place are highlighted by different colours. (e) Time-derivative curves for sample with regular oxygen content, scaled by the respective maximum length changes and time constants obtained from kinetic fitting, in order to distinguish between the formation regions of $\omega_{dl,iso}$ and ω_{iso} (Color figure online).

In contrast, in the temperature range above 250 °C, where ω_{iso} -formation takes place *predominantly*, the process is found to be faster in case of the sample with regular oxygen content. As described in Section I, ω_{iso} -formation starts in regions, which get depleted in V by an underlying decomposition process. The tendency to decompose seems to be a function of the oxygen content, *i.e.*, increasing oxygen contents

promote decomposition, as can be deduced from Figure 1. Here, the decomposition region only shows up for alloys containing a finite amount of oxygen (red dash-dotted lines), but no such region is present for the phase diagram predicted for an oxygen-free sample (black lines). Thus, in case of the sample with an increased oxygen content, decomposition should proceed faster and/or to a higher extent making

the faster progression of ω_{iso} -formation comprehensible.

For the sample with a reduced oxygen content, the length increase observed in case of ageing at 400 °C is hardly visible and no length increase at all appears in case of ageing at 450 °C indicating α -phase formation to occur strongly reduced. The oxygen content is known to strongly influence the ω -to- α -transformation, but in a non-linear, complex way.^[23]

3. V-content of omega-phase particles after long-term ageing

The distinct length changes due to ω -formation yields access to the V-content $c_{V,\omega}$ of the ω -phase provided its phase fraction (x_ω) is known (see Eq. [2] and Figure 4(a)). This is a valuable piece of additional information that can be extracted from the dilatometric data since V-concentrations of the ω -phase formed at low ageing temperatures has not been accessible so far due to the minute size of the particles and potentially small compositional variations with respect to the surrounding matrix there.

An ω -phase fraction of *ca.* 67 mol pct is reported from studies by analytical transmission electron microscopy after longtime ageing (10 days) at T_{amb} ^[17], a fraction of *ca.* 50 mol pct is reported after ageing at 300 °C.^[24] Therefore, the final ω -phase fraction for all ageing temperatures in between T_{amb} and 300 °C in the present studies can be assumed to be in the range between 50 and 67 mol pct.

The final total length changes A due to ω -formation are obtained by extrapolating the measuring data using the kinetic model presented in the next section (Section IV). With these total length changes A , the V-concentrations $c_{V,\omega}^{f,50}$ and $c_{V,\omega}^{f,67}$ of the ω -phase particles present after long-term ageing can be calculated by means of Eq. [2] for the two phase fractions x_ω quoted above. The values are listed in Table I.

IV. KINETIC MODELLING

A. Application of the Austin–Rickett Kinetic Model

In this section, the Austin–Rickett (AR) kinetic model,^[25] a modified version of the

Johnson–Mehl–Avrami–Kolmogorov (JMAK) model is applied to analyse the dilatometric data obtained for ω -formation, *i.e.*, for the measurements in the temperature range up till 350 °C. From the model, temperature-dependent phase formation rates and in further sequence TTT-diagrams can be derived, which are indispensable ingredients for many aspects of materials research in this area. Reasoning why the AR model is better suited for describing the ω -formation in the present Ti–V-alloy than the JMAK-model is given in Appendix B.

The AR-kinetic model yields for the fraction $\alpha(t)$ of new phase^[25]:

$$\alpha(t) = 1 - \frac{1}{(k(T)t)^{n_{AR}} + 1}, \quad [4]$$

where $k(T)$ is the temperature-dependent rate of the process and n_{AR} a factor alike the Avrami-exponent.^[26] Equation [4] is applied to fit the length change variation upon annealing by means of the fit function

$$f(t) = A\alpha(t) + f_0 = A \left\{ 1 - \frac{1}{(k(T)t)^{n_{AR}} + 1} \right\} + f_0, \quad [5]$$

where A denotes the maximum length change and an f_0 initial y-distance.

The numerical results of fitting the measured relative changes by means of the MatLab routine *nlinfit* are listed in Table II. For selected temperatures, the fitted length change curves are shown in Figure 6. The plots on the logarithmic time scale underline that the experimental data can be well described by the kinetic model.

B. Discussion of Fitting Results

1. Variation of exponent with temperature

Figure 7(a) shows the variation of the exponent n_{AR} with temperature according to the fit results of Table II. An increase of n_{AR} with temperature can be discerned for both samples with the increase of the sample with strongly reduced oxygen content being shifted to higher temperatures.

The exponent n_{AR} is known to increase both with the nucleation rate and the dimensionality of the growth process.^[26] The small n_{AR} -values for reduced ageing

Table I. Final V-contents $c_{V,\omega}^{f,50}$ and $c_{V,\omega}^{f,67}$ of the ω -Phase Particles Upon Long-Term Ageing at the Quoted Temperature T_a Deduced by Means of Eq. [2] from the Total Length Change A for the ω -Phase fraction of 50 and 67 mol pct

| T_a [°C] | Ti20.9V | | | Ti21.3V (HP) | | |
|------------|-------------------|---------------------------------|---------------------------------|-------------------|---------------------------------|---------------------------------|
| | A [10^{-3}] | $c_{V,\omega}^{f,50}$ [mol pct] | $c_{V,\omega}^{f,67}$ [mol pct] | A [10^{-3}] | $c_{V,\omega}^{f,50}$ [mol pct] | $c_{V,\omega}^{f,67}$ [mol pct] |
| 41 | − 0.09 | 14.0 | 14.1 | — | — | — |
| 80 | − 0.36 | 12.1 | 12.5 | — | — | — |
| 100 | − 0.71 | 10.1 | 10.9 | − 0.80 | 9.6 | 10.5 |
| 150 | − 0.88 | 9.2 | 10.2 | − 1.02 | 8.6 | 9.6 |
| 200 | − 1.14 | 8.0 | 9.2 | − 1.27 | 7.5 | 8.7 |
| 250 | − 1.57 | 6.3 | 7.7 | − 1.61 | 6.2 | 7.5 |
| 300 | − 1.88 | 5.2 | 6.8 | − 1.98 | 4.9 | 6.4 |

Table II. Numerical Results of Fitting the Measured Relative Changes (Fig. 3) with Austin–Rickett kinetic Model (Eq. [5]) of Sample with Regular (Ti20.9V) and with Strongly Reduced Oxygen Content (Ti21.3V(HP)) for Ageing Temperature (T_a) Regime of ω -Phase Formation

| T_a (°C) | Ti20.9V | | | Ti21.3V (HP) | | |
|------------|-------------------|-----------------------|----------|-------------------|-----------------------|----------|
| | A [10^{-3}] | k [s^{-1}] | n_{AR} | A [10^{-3}] | k [s^{-1}] | n_{AR} |
| 41 | −0.09 | 7.21×10^{-7} | 0.51 | — | — | — |
| 80 | −0.36 | 9.89×10^{-7} | 0.68 | — | — | — |
| 100 | −0.71 | 1.02×10^{-6} | 0.87 | −0.80 | 8.44×10^{-6} | 0.57 |
| 150 | −0.88 | 2.26×10^{-5} | 0.83 | −1.02 | 4.19×10^{-5} | 0.81 |
| 200 | −1.14 | 6.31×10^{-5} | 1.20 | −1.27 | 1.03×10^{-4} | 0.92 |
| 250 | −1.57 | 2.28×10^{-4} | 1.28 | −1.61 | 2.19×10^{-4} | 0.91 |
| 300 | −1.88 | 3.12×10^{-4} | 1.58 | −1.98 | 2.45×10^{-4} | 1.32 |
| 350 | −1.71 | 4.89×10^{-5} | 1.84 | −1.84 | 2.31×10^{-5} | 1.51 |

A : maximum length change, k : rate, n_{AR} : exponent. For selected temperatures, fit results are shown in Fig. 6

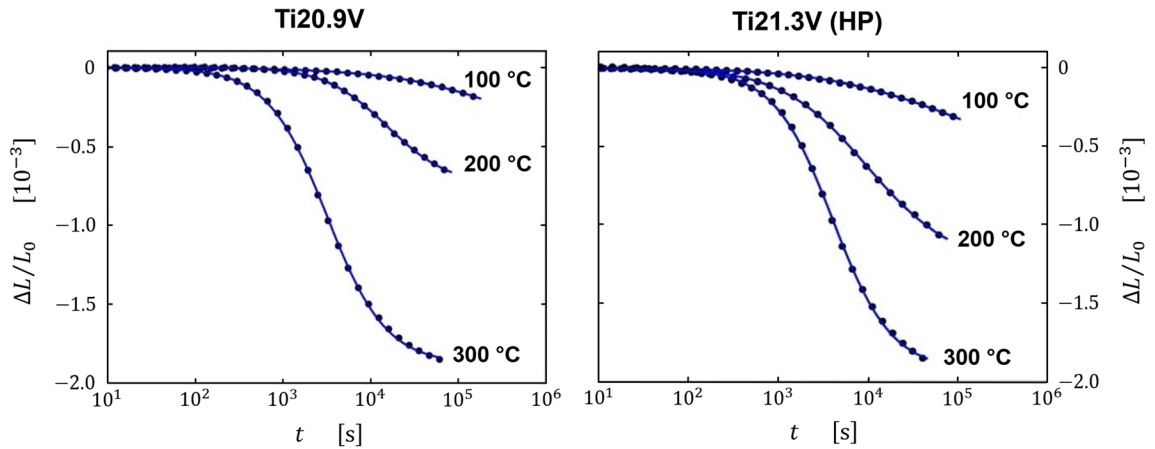


Fig. 6—Fitting relative changes with Austin–Rickett kinetic model according Eq. [5] for selected ageing temperatures of sample with regular (left) and with strongly reduced oxygen content (right). Measuring data (identical to those in Fig. 3): black filled circles; fit: blue curves. Logarithmic time scale is used in order to make the quality of the regression apparent (Color figure online).

temperatures indicate a low nucleation rate and reduced dimensionality of the growth process. This can be well understood since by quenching to low ageing temperatures, *i.e.*, close to the athermal transformation limit T_{ath} for the average composition, the alloy becomes more unstable compared to quenching and ageing at elevated temperatures. This is rooted in the presence of nano-scale regions low in vanadium which arise as a consequence of quenched in compositional fluctuations. Those regions are already below their local T_{ath} at low annealing temperatures and can transform in time through the diffusionless-isothermal mechanism.^[17] In this picture the potential nucleation sites for the formation are already present and a classical nucleation process does not occur. Furthermore, the ω -phase particles are known to remain nanoscale upon ageing at low temperatures, *i.e.*, to grow only slightly or not at all. As a consequence, the dimensionality of growth should be close to zero.

Conversely, upon ageing at elevated temperatures, the nucleation rate is higher due to the ongoing decomposition process which is steadily providing new V-lean

regions where ω -phase nuclei can be formed. Furthermore, even though the particles stay small, notable growth is known to occur resulting in ellipsoid particle shapes,^[5] and thus in a larger value of dimensionality of the growth process compared to low temperature ageing.

It is worthwhile to mention the slight plateau occurring upon increase of n_{AR} in the range of 150 C or around 200 °C. Remarkably, this is the temperature range where the transition from the $\omega_{dl,iso}$ - to the ω_{iso} -formation takes place. Hence, the results of this section represent further building blocks of a consistent picture of the different modes of ω -formation.

2. Isothermal TTT-diagram

Figure 7(b) shows the isothermal TTT-diagram that has been calculated from the fit results of the AR-kinetic model (Table II). The points mark a length change of 50 pct of the total length change caused by ω -formation characterising the progress of phase formation with respect to phase fraction formed and degree of decomposition achieved. The diagram clearly shows that in the

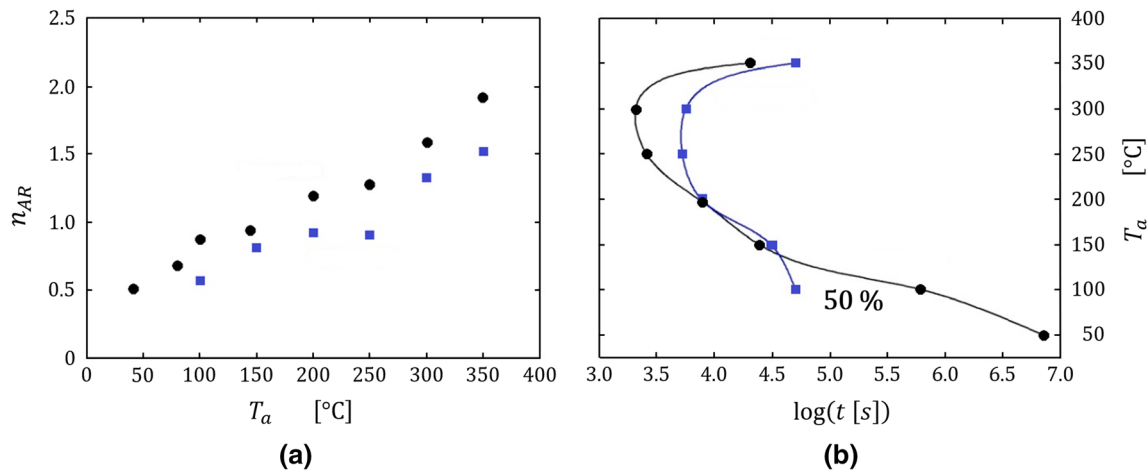


Fig. 7—(a) Exponent n_{AR} of Austin–Rickett kinetic model (Eq. [5]) in dependence of aging temperature T_a according to the fit results of Table II. (b). Isothermal TTT-diagram for time t required for 50 pct of total length change to occur as deduced from the fitted data (Table II). Temperature regime of ω -phase formation. Black coloured dots: sample with regular oxygen content (Ti20.9V); blue-coloured squares: sample with strongly reduced oxygen content (Ti21.3V(HP)) (Color figure online).

temperature range from 200 °C to 350 °C, ω -formation is promoted by the higher amount of oxygen. As discussed in Section III–C, a likely explanation for this behaviour is the stronger tendency for decomposition, compared to alloys with lower oxygen contents, in the temperature range of ω_{iso} -formation.

For temperatures beneath 200 °C, the TTT-curve shows a bulge-like behaviour for the sample with a regular oxygen content for 150 °C. In case of the sample with a strongly reduced oxygen content, bending of the curve is observed at this temperature, which may even grow into a bulge at lower temperatures. Similar results have been obtained by DSC-measurements.^[22] Here, a larger bulge shifted to lower temperatures was found for reduced oxygen content, indicating the increased formation of the $\omega_{dl,iso}$ -phase due to a higher nucleation rate.

V. SUMMARY AND CONCLUSION

The present work extends the available toolbox of investigation methods for examining phase formation and transformation processes in β -stabilised Ti-alloys by the technique of dilatometry. Two Ti-alloys, each with about 21 at. pct V but with different oxygen contents, have been examined, which were subjected to heat treatment consisting of solution annealing, quenching, and isothermal ageing at various temperatures.

Formulae have been developed, which allow to calculate sample length changes occurring as a result of varying phase fractions and compositions during these formation and transformation processes. Based on that, from the presented length change measurements, qualitative and quantitative conclusions on these processes could be derived, the most prominent ones can be summarized as follows:

1. The basic processes being at work in the temperature range investigated are diffusionless and

diffusion-assisted isothermal ω -formation as well as ω -to- α -transformation, for which the phase regions have been localised for both samples. For both samples, ω is formed *via* the diffusionless mechanism for $T \leq 200$ °C and *via* the diffusion-assisted one for $T \geq 200$ °C. For $T \geq 400$ °C, ω -to- α -transformation is observed.

2. By making use of the dilatometric measurements and ω -phase fractions from literature, the average composition of ω -phase particles present after long-term isothermal ageing were successfully evaluated for their entire formation range. For both samples, their final V-content has been found to decrease with increasing temperature.
3. In particular, the influence of a varying oxygen content on ω -formation kinetics could clearly be resolved. Low oxygen contents promote the diffusionless ω -formation mechanism, but retard the diffusion-assisted one as well as the ω -to- α -transformation process.

Kinetic modeling of the dilatometric measurements conducted in the temperature range of ω -phase formation has been performed:

4. The application of the AR-kinetic model to the measurements has been validated. By fitting this model to the measurements obtained, the temperature-dependent rates were determined and, on their basis, part of the isothermal TTT-diagram was developed. Herein, the influence of the oxygen content becomes visible in accordance with the former conclusions.

The present work lays the basis for further studies of ω -formation and transformation processes in Ti-alloys. Preliminary experiments with Ti-alloys containing other β -stabilisers indicate similar length change characteristics. The evaluation method developed in this work

enables a full characterisation of the underlying processes. Such studies, therefore, may lead to a complete picture of ω -phase formation in Ti-alloys and a more extensive understanding of its nature.

APPENDIX A: FORMULA OF LENGTH CHANGES ASSOCIATED WITH TRANSFORMATION PROCESSES

In the following section, the formula which were used in Section III–B for the relative length changes associated with decomposition (Eq. [1]), ω -phase formation (Eq. [2]), and ω -to- α -transformation (Eq. [3]) will be derived.

The length changes associated with these processes are derived

- ... assuming a homogeneous initial β -phase right after quenching with V-concentration c_0 and average atomic volume v_0 ,
- ... considering the formation of several phases, each with a mole fraction x_{pi} and an average atomic volume v_{pi} ,
- ... taking into consideration that the atomic volume v_{pi} depend on the V-content $c_{V,pi}$ and on the temperature T .

In order to calculate the length changes based on the volumetric changes, the common approximation $\Delta L/L_0 \approx 1/3(\Delta V/V_0)$ is applied. This relation holds for isotropic samples and length changes, which are by several orders of magnitude smaller than the sample length. Summing up the relative volumetric changes caused by the freshly formed phases with respect to the initial atomic volume weighted by their respective phase fractions yields:

$$\frac{\Delta L}{L_0} \approx \frac{1}{3} \frac{\Delta V}{V_0} = \frac{1}{3} x_{p1} \frac{v_{p1}(c_{V,p1}, T) - v_0}{v_0} + \frac{1}{3} x_{p2} \frac{v_{p2}(c_{V,p2}, T) - v_0}{v_0} + \dots \quad [\text{A1}]$$

Between the phase fractions and the V-concentration in the various phases, the following conditions hold:

$$x_{p1} + x_{p2} + \dots = 1, \quad [\text{A2a}]$$

$$x_{p1} c_{V,p1} + x_{p2} c_{V,p2} + \dots = c_0. \quad [\text{A2b}]$$

The three processes mentioned above are considered:

- Decomposition of the quenched in β -phase in V-rich and V-lean parts ($\beta_Q \rightarrow \beta_l + \beta_r$) with corresponding atomic volumes v_{β_l} , v_{β_r} , mole fractions x_{β_l} , x_{β_r} , and V-concentration c_{V,β_l} , c_{V,β_r} .

- ω -phase formation: $\beta_Q \rightarrow \omega + \beta_r$, with corresponding atomic volumes v_ω , v_{β_r} , phase fractions x_ω , x_{β_r} , and V-concentrations $c_{V,\omega}$, c_{V,β_r} .
- ω -to- α -transformation: $\beta_r + \omega \rightarrow \beta_r + \alpha + \omega$, with corresponding atomic volumes v_{β_r} , v_ω , v_α , phase fractions x_{β_r} , x_ω , x_α , and V-concentrations $c_{V,\omega}$, c_{V,β_r} .

The temperature variation of the lattice constants with respect to the value at ambient temperature T_{amb} is taken into consideration by a factor $\gamma(c_V, T)$ which is based on Vegard's rule^[27] and the expansion coefficients of pure Ti and V^[28,29]:

$$\gamma(c_V, T) = 1 + (1 - c_V) \int_{T_{amb}}^T \alpha_{Ti}(\tilde{T}) d\tilde{T} + c_V \int_{T_{amb}}^T \alpha_V(\tilde{T}) d\tilde{T}. \quad [\text{A3}]$$

Decomposition Upon decomposition V-lean (β_l) and V-rich regions (β_r) are formed, while the entire sample remains in the β -phase. The lattice constant a_β of the β -phase is known to linearly increase with decreasing V-content^[30]:

$$a_\beta(c_V, T)[\text{Å}] = \gamma(c_V, T) \{3.282 - 2.57 \times 10^{-3} c_V[\text{at.pct}]\}, \quad [\text{A4}]$$

where the factor $\gamma(c_V, T)$ (Eq. [A3]) has been added to account for thermal expansion. The atomic volume is related to $a_\beta(c_V, T)$ as follows

$$v_\beta = \frac{1}{2} a_\beta^3(c_V, T), \quad [\text{A5}]$$

taking into account the number of atoms per unit cell of β -phase. In the case of mere decomposition taking place, Eq. [A1] turns into

$$\begin{aligned} \left(\frac{\Delta L}{L_0}\right)_{\text{decomp.}} &\approx \frac{1}{3} \left(\frac{\Delta V}{V_0}\right)_{\text{decomp.}} \\ &= \frac{1}{3} x_{\beta_l} \left(\frac{v_{\beta_l}(c_V, T)}{v_{\beta,0}} - 1\right) \\ &\quad + \frac{1}{3} x_{\beta_r} \left(\frac{v_{\beta_r}(c_V, T)}{v_{\beta,0}} - 1\right) \\ &= \left(\frac{\Delta L}{L_0}\right)_{\beta_l} + \left(\frac{\Delta L}{L_0}\right)_{\beta_r}, \end{aligned} \quad [\text{A6}]$$

with the atomic volumes according to Eq. [A5] in combination with Eqs. [A4] and [A3]. In between the fractions and compositions, the relations

$$x_{\beta_l} + x_{\beta_r} = 1 \quad [\text{A7a}]$$

and

$$c_{V,\beta_l} x_{\beta_l} + c_{V,\beta_r} x_{\beta_r} = c_0. \quad [\text{A7b}]$$

hold according to Eq. [A2]. Substituting in Eq. [A6] the atomic volumes by the respective lattice constants yields Eq. [1] used in Section III–B.

Omega-formation For calculating the length change associated with the ω -formation, we start with considering the atomic volume of this phase. The lattice constants a_ω and c_ω of the hexagonal ω -phase are functions of the V-content. Based on the data provided by Aurelio *et al.*,^[30] the following quadratic relations are obtained

$$a_\omega(c_V, T)[\text{Å}] = \gamma(c_V, T) \{4.6100 - 1.0250 \times 10^{-4} c_V^2 [\text{at.pct}]\}, \quad [\text{A8a}]$$

$$c_\omega(c_V, T)[\text{Å}] = \gamma(c_V, T) \{2.8170 - 0.3544 \times 10^{-4} c_V^2 [\text{at.pct}]\}, \quad [\text{A8b}]$$

where the factor $\gamma(c_V, T)$ (Eq. [A3]) again accounts for the thermal expansion. The average atomic volume in the hexagonal ω -phase is given by

$$v_\omega(c_V, T) = \frac{1}{3} \frac{\sqrt{3}}{2} a_\omega^2(c_V, T) c_\omega(c_V, T), \quad [\text{A9}]$$

taking into account the number of atoms per unit cell of β -phase. For the atomic volume of the β -matrix Eq. [A5] holds as given above. With these atomic volumes, Eq. [A1] for the length change due to ω -phase formation reads:

$$\begin{aligned} \left(\frac{\Delta L}{L_0}\right)_{\omega\text{-form.}} &\approx \frac{1}{3} \left(\frac{\Delta V}{V_0}\right)_{\omega\text{-form.}} \\ &= \frac{1}{3} x_\omega \left(\frac{v_\omega(c_V, T)}{v_{\beta,0}} - 1\right) \\ &\quad + \frac{1}{3} x_{\beta_r} \left(\frac{v_{\beta_r}(c_V, T)}{v_{\beta,0}} - 1\right) \\ &= \left(\frac{\Delta L}{L_0}\right)_\omega + \left(\frac{\Delta L}{L_0}\right)_{\beta_r}. \end{aligned} \quad [\text{A10}]$$

The relations between the fractions and compositions (Eq. [A2]) are in this case given by:

$$x_\omega + x_{\beta_r} = 1 \quad [\text{A11a}]$$

and

$$c_{V,\omega} x_\omega + c_{V,\beta_r} x_{\beta_r} = c_0. \quad [\text{A11b}]$$

Again by substituting in Eq. [A10] the atomic volumes by the respective lattice constants, Eq. [2] is obtained that is used in Section III–B.

Omega-to-alpha transformation For calculating the length change upon ω -to- α -transformation, we first consider the atomic volume of the emerging hexagonal α -phase. Since the α -phase shows only insignificant solubility for vanadium,^[31,32] its lattice constants^[33] are assumed to be independent of the V-content. They vary only as a function of temperature due to thermal expansion according to:

$$a_\alpha(T) = \gamma(c_V = 0, T) \times 2.95111 \text{ Å} \quad [\text{A12a}]$$

and

$$c_\alpha(T) = \gamma(c_V = 0, T) \times 4.68433 \text{ Å}. \quad [\text{A12b}]$$

The atomic volume of the α -phase is obtained from Eq. [A9] using as pre-factor 1/2 instead of 1/3, due to the different number of atoms per unit cell compared to the hexagonal ω -phase. The atomic volumes of the β -phase and the ω -phase are given by Eqs. [A5] and [A9], respectively.

The starting configuration for the ω -to- α -transformation is composed of V-lean ω -phase particles with molar fraction x_ω^0 and V-content $c_{V,\omega}^0$ embedded in a V-enriched β -phase matrix with phase fraction x_{β_r} and V-content c_{V,β_r} . Upon transformation the fraction x_α of the α -phase increases on expense of the fraction the ω -phase. In this case, Eq. [A1] for the length change turns into:

$$\begin{aligned} \left(\frac{\Delta L}{L_0}\right)_{\omega\text{-to-}\alpha\text{-transform.}} &\approx \frac{1}{3} \left(\frac{\Delta V}{V_0}\right)_{\omega\text{-to-}\alpha\text{-transform.}} \\ &= \frac{1}{3} x_\alpha \left(\frac{v_\alpha(c_V, T)}{v_{\beta,0}} - 1\right) \\ &\quad + \frac{1}{3} (x_\omega^0 - x_\alpha) \left(\frac{v_\omega(c_V, T)}{v_{\beta,0}} - 1\right) \\ &\quad + \frac{1}{3} x_{\beta_r} \left(\frac{v_{\beta_r}(c_V, T)}{v_{\beta,0}} - 1\right) \\ &= \left(\frac{\Delta L}{L_0}\right)_\alpha + \left(\frac{\Delta L}{L_0}\right)_\omega + \left(\frac{\Delta L}{L_0}\right)_{\beta_r}. \end{aligned} \quad [\text{A13}]$$

In between the fractions and compositions, the relations

$$x_\omega + x_\alpha + x_{\beta_r} = 1 \quad [\text{A14a}]$$

and

$$c_{V,\omega}^0 x_\omega + c_{V,\beta_r} x_{\beta_r} = c_0. \quad [\text{A14b}]$$

hold according to Eq. [A2] along with a further condition accounting for the fact, that α -phase particles form only by transformation of initially present α -phase particles:

$$x_\omega + x_\alpha = x_\omega^0. \quad [\text{A14c}]$$

Substituting in Eq. [A13] again the atomic volumes by the respective lattice constants yields Eq. [3] used in Section III–B.

APPENDIX B: CHOICE OF KINETIC MODEL

In the following, reasoning is outlined why the AR model is better suited for describing the ω -formation in the present Ti–V-alloy than the JMAK-model.

In the AR model, the temporal change $\dot{\alpha}$ of the phase fraction α is proportional to $(1 - \alpha)^2$,^[25] whereas for the JMAK-model a linear relation holds ($\dot{\alpha} \propto (1 - \alpha)$). Therefore, in the AR model $\dot{\alpha}$ decreases stronger in the beginning and weaker towards the end compared to the case of the JMAK-model. Just, this model feature is needed to take into account a larger impingement in the ω -formation process.

Impingement at objects other than neighbouring domains of the product phase is considered negligible for JMAK kinetics,^[34] which is not the case for ω -formation. In fact, after their formation, ω -phase particles eject V-atoms into their immediate surroundings exchanging them by Ti-atoms. In doing so, the surrounding matrix is stabilised in its β -phase. As a result, the growth of ω -phase particles does not only get impeded by other ω -phase particles but also by the matrix material.

A further idealisation underlying JMAK kinetics^[34] fails for ω -formation, namely that nuclei are randomly distributed and growth rates are independent of the position in the sample. The activation energy to perform the initial collapse necessary for ω -phase formation is broadly distributed.^[22] This is caused by differences in the V-content of these regions and by large lattice tensions accompanying compositional differences in the Ti–V-system. Furthermore, due to variations in the composition of the immediate surroundings of the ω -phase particles, subsequent growth may either appear more slowly or rapidly.

To sum up, the need for a stronger impingement and thus application of AR-kinetic model can be argued well by not meeting certain idealisations of the JMAK-model.

ACKNOWLEDGMENTS

This work was performed in the framework of the interuniversity cooperation of TU Graz and Uni Graz on natural sciences (NAWI Graz). Support by the GIMRT Program of the Institute for Materials Research, Tohoku University (Grant No. 19K0513) is gratefully acknowledged.

CONFLICT OF INTEREST

The authors declare that they have no conflict of interest.

FUNDING

Open access funding provided by Graz University of Technology.

OPEN ACCESS

This article is licensed under a Creative Commons Attribution 4.0 International License, which permits use, sharing, adaptation, distribution and reproduction

in any medium or format, as long as you give appropriate credit to the original author(s) and the source, provide a link to the Creative Commons licence, and indicate if changes were made. The images or other third party material in this article are included in the article's Creative Commons licence, unless indicated otherwise in a credit line to the material. If material is not included in the article's Creative Commons licence and your intended use is not permitted by statutory regulation or exceeds the permitted use, you will need to obtain permission directly from the copyright holder. To view a copy of this licence, visit <http://creativecommons.org/licenses/by/4.0/>.

REFERENCES

1. C. Leyens and M. Peters: *Titanium and Titanium Alloys: Fundamentals and Applications*, 1st ed., Wiley, Hoboken, 2003.
2. M. Kaur and K. Singh: *Mater. Sci. Eng. C*, 2019, Vol. 102, pp. 844–62.
3. J.C. Williams and R.R. Boyer: *Metals*, 2020, Vol. 10, p. 705.
4. R.P. Kolli and A. Devaraj: *Metals*, 2018, Vol. 8, p. 506.
5. B. Hickman: *J. Mater. Sci.*, 1969, Vol. 4, pp. 554–63.
6. S. Sikka, Y. Vohra, and R. Chidambaram: *Prog. Mater. Sci.*, 1982, Vol. 27, pp. 245–310.
7. S. Nag, R. Banerjee, R. Srinivasan, J. Hwang, M. Harper, and H. Fraser: *Acta Mater.*, 2009, Vol. 57, pp. 2136–47.
8. M. Tane, T. Nakano, S. Kuramoto, M. Hara, M. Niinomi, N. Takesue, T. Yano, and H. Nakajima: *Acta Mater.*, 2011, Vol. 59, pp. 6975–88.
9. A. Devaraj, V.V. Joshi, A. Srivastava, S. Manandhar, V. Moxson, V.A. Duz, and C. Lavender: *Nat. Commun.*, 2016, Vol. 7, pp. 1–8.
10. M. Luckabauer, W. Sprengel, and R. Würschum: *Rev. Sci. Instrum.*, 2016, Vol. 87, p. 075116.
11. R. Würschum, R. Enzinger, E. Hengge, and W. Sprengel: *IOP Conf. Ser. Mater. Sci. Eng.*, 2019, Vol. 580, p. 012502.
12. E. Hengge, R. Enzinger, M. Luckabauer, W. Sprengel, and R. Würschum: *Philos. Mag. Lett.*, 2018, Vol. 98, pp. 301–09.
13. R. Enzinger, E. Hengge, W. Sprengel, and R. Würschum: *J. Mater. Sci.*, 2019, Vol. 54, pp. 5083–91.
14. J. Williams, B. Hickman, and D. Leslie: *Metall. Trans.*, 1971, Vol. 2, pp. 477–84.
15. Y. Xia, J. Zhao, Q. Tian, and X. Guo: *J. Min. Met. Mater. Soc.*, 2019, Vol. 71, pp. 3209–3220.
16. G. Lindwall, P. Wang, U.R. Kattner, and C.E. Campbell: *J. Min. Met. Mater. Soc.*, 2018, Vol. 70, pp. 1692–1705.
17. M. Tane, H. Nishiyama, A. Umeda, N.L. Okamoto, K. Inoue, M. Luckabauer, Y. Nagai, T. Sekino, T. Nakano, and T. Ichitsubo: *Phys. Rev. Mater.*, 2019, Vol. 3, p. 043604.
18. N.L. Okamoto, S. Kasatani, M. Luckabauer, R. Enzinger, S. Tsutsui, M. Tane, and T. Ichitsubo: *Phys. Rev. Mater.*, 2020, Vol. 4, p. 123603.
19. D. De Fontaine, N. Paton, and J. Williams: *Acta Metall.*, 1971, Vol. 19, pp. 1153–62.
20. A. Devaraj, S. Nag, R. Srinivasan, R. Williams, S. Banerjee, R. Banerjee, and H. Fraser: *Acta Mater.*, 2012, Vol. 60, pp. 596–609.
21. R.J. Enzinger, M. Luckabauer, T. Ichitsubo, and R. Würschum: *Mater. Sci. Forum*, 2021, Vol. 1016, pp. 1851–56.
22. N.L. Okamoto, S. Kasatani, M. Luckabauer, M. Tane, and T. Ichitsubo: *Scr. Mater.*, 2020, Vol. 188, pp. 88–91.
23. K. Chou and E.A. Marquis: *Acta Mater.*, 2019, Vol. 181, pp. 367–76.
24. M. Hendrickson: The role of misfit strain and oxygen content on formation and evolution of omega precipitate in metastable beta-titanium alloys, Dissertation, University of North Texas, Denton, TX, December 2016.
25. J. Austin and R. Rickett: *Trans. AIME*, 1939, Vol. 135, pp. 396–415.
26. M. Starink: *J. Mater. Sci.*, 2001, Vol. 36, pp. 4433–41.
27. L. Vegard: *Z. Phys.*, 1921, Vol. 5, pp. 7–26.
28. P. Hidnert: *J. Res. NIST*, 1943, Vol. 30, p. 101.

29. Y.M. Kozlovskii and S. Stankus: *J. Phys. Conf. Ser.*, 2000, Vol. 1677, p. 012167.
30. G. Aurelio, A.F. Guillermet, G. Cuello, and J. Campo: *Metall. Mater. Trans. A*, 2002, Vol. 33A, pp. 1307–317.
31. V. Molokanov, D. Chernov, and P. Budberg: *Met. Sci. Heat Treat.*, 1997, Vol. 19, pp. 704–05.
32. H. Adenstedt, J. Pequignot, and J. Raymer: *Trans. Am. Soc. Met.*, 1952, Vol. 44, pp. 990–1003.
33. R. Wood: *Proc. Phys. Soc.*, 1962, Vol. 80, p. 783.
34. F. Cumbreira and F. Sanchez-Bajo: *Thermochim. Acta*, 1955, Vol. 266, pp. 315–30.

Publisher's Note Springer Nature remains neutral with regard to jurisdictional claims in published maps and institutional affiliations.